PCCP

ROYAL SOCIETY OF CHEMISTRY

PAPER

View Article Online
View Journal | View Issue

Check for updates

Cite this: *Phys. Chem. Chem. Phys.*, 2025, **27**, 861

An orbital-overlap complement to σ-hole electrostatic potentials†

Arshad Mehmood *[a] and Benjamin G. Janesko [b]

Received 7th October 2024,
Accepted 3rd December 2024

DOI: 10.1039/d4cp03851g

rsc.li/pccp

A σ-hole is an electron-deficient region of positive electrostatic potential (ESP) opposite from a half-filled p orbital involved in forming a covalent bond. The σ-hole concept helps rationalize directional noncovalent interactions, known as σ-hole bonds, between covalently bonded group V–VII atoms and electron-pair donors. The magnitude and orientation of σ-holes are correlated with the strength and geometry of halogen bonds. However, ESP computed for isolated σ-holes are not always predictive of *interaction* energies. For example, the σ-holes of isolated $CHFBr_2$ and isolated CH_2FI have identical ESP on the molecule surface, but halogen bonds to these molecules generally have different strengths. Here we show that the compact/diffuse nature of the orbitals involved plays an important role. Our orbital overlap distance quantifies the compact/diffuse nature of the "test orbital" that best overlaps with a systems orbitals at each point. The overlap distance captures the response properties of σ-holes: diffuse σ-holes with large overlap distance are typically "softer" and more polarizable. This aids visualization and interpretation. A linear fit to overlap distance and ESP is predictive of the halogen bond strengths of CH_3X and CF_3X (X = Cl, Br and I). We suggest that the overlap distance will be a useful partner to ESP for characterizing σ-holes.

1. Introduction

In 1992, Brinck *et al.*[1] reported that the molecular electrostatic potential (ESP) around the halogen atom in haloalkanes is not isotropic but shows regions of positive and negative values. The positive region is localized in the elongation of the C–X (X = Cl, Br, I) covalent bond while the negative ESP is found as a concentric belt around the C–X (Fig. 1).[1,2] The positive region is referred to as the "σ-hole" and is attributed to the electron-deficient outer lobe of the halogen p orbital involved in forming the covalent bond.[2,3] The σ-hole has been advanced as an explanation for halogen bonding.[4–6] Halogen bonds are directional noncovalent interactions between a halogen and an electron donor, which were identified experimentally decades before reports of σ-holes.[2,7–10] The magnitudes of σ-holes are typically quantified as the maximum value of ESP in the σ-hole region, $V_{S,max}$, evaluated on a molecular density isosurface.[2,7] Several reports[7,11–14] demonstrate that halogen bond strengths often correlate well with $V_{S,max}$, and with the corresponding electrostatic potential minimum of σ-hole acceptors (electron-pair donors). Halide σ-hole $V_{S,max}$ generally increases with increasing polarizability and decreasing electronegativity F < Cl < Br < I.[15] The magnitude of $V_{S,max}$ also increases as the alkyl portion C–X becomes more electron-withdrawing.[16]

Response properties are an important aspect of σ-hole chemistry. Systematic studies show that $V_{S,max}$ computed for isolated σ-holes do not always capture halogen bond interaction strengths.[17–23] Fig. 1 shows a simple example: while

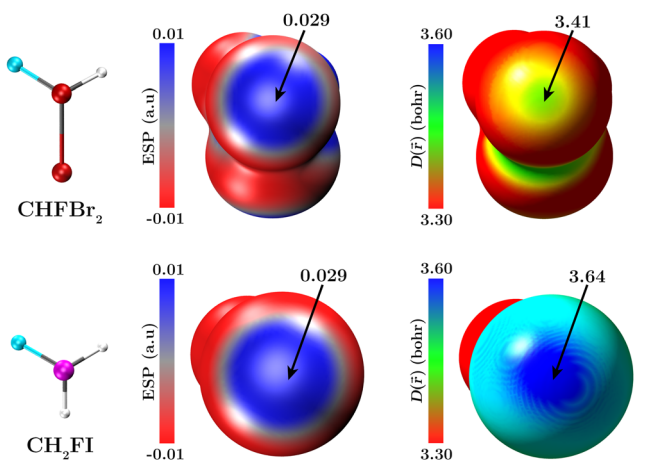

Fig. 1 σ-holes on $CHFBr_2$ and CH_2FI molecules. (left) Molecule structure (middle-right) molecular ESP and $D(\vec{r})$ plotted on the 0.001 e bohr^{-3} electron density isosurface.

[a] *Division of Information Technology – Research Computing, Informatics & Innovation and Institute for Advanced Computational Science, Stony Brook University, Stony Brook, New York 11794, USA. E-mail: arshad.mehmood@stonybrook.edu; Tel: +1 631-632-2340*

[b] *Department of Chemistry & Biochemistry, Texas Christian University, Fort Worth, Texas 76129, USA*

† Electronic supplementary information (ESI) available: Applications to group IV–VI elements, and transition metal clusters. See DOI: https://doi.org/10.1039/d4cp03851g

isolated $CHFBr_2$ and isolated CH_2FI have identical $V_{S,max}$, the more polarizable iodine forms a stronger halogen bond to ammonia ($CHFBr_2$ = −2.91 kcal mole^{-1}, CH_2FI = −3.22 kcal mole^{-1}, MP2/aug-cc-pVTZ results). Murray *et al.*[17] highlighted that $V_{S,max}$ computed for free molecules, fail to account for the polarization of charge distributions induced by interacting molecules. Clark *et al.*[18] reported that $V_{S,max}$ of isolated halogen bond donors X_3C–I, X = F, Cl, Br did not always correlate with computed halogen bond energies, and discussed the discrepancy in terms of polarization.[21] Duarte *et al.*[19] reported that $V_{S,max}$ of isolated halogen bond acceptors did not always correlate with computed halogen bond energies for F–Br···X–R, X = F, Cl, Br, I and R = –H, –F. These discrepancies have also been attributed to orbital or charge-transfer effects.[20,22,24–37] These discussions are controversial.[21,23,38–47] Several studies have instead focused on the practical question of whether the combination of ESP at an isodensity surface and other properties, computed for isolated σ-hole donors and acceptors, can improve the qualitative understanding and quantitative prediction of halogen bond strength. Tested properties include local ionization energies, local surface electron attachment energies, natural bond orbital analysis, and others.[9,26,48–50] To date, there appears no general consensus on the "best' complement to ESP.

Here we explore our orbital overlap distance $D(\vec{r})$ as a new complement to ESP. $D(\vec{r})$ is built from the expectation value of a nonlocal one-electron operator, a normalized hydrogenic "test function" $C_d \exp\left(-|\vec{r}-\vec{r}'|^2/d^2\right)$, $C_d = \left[2/(\pi d^2)\right]^{3/4}$ centered at point $\vec{r}$ and having width d. We define

$$EDR(\vec{r};d) = \rho^{-\frac{1}{2}}(\vec{r})\int d^3\vec{r}'\gamma(\vec{r},\vec{r}')C_d \exp\left(-\frac{|\vec{r}-\vec{r}|^2}{d^2}\right). \quad (1)$$

The one-particle density matrix $\gamma(\vec{r},\vec{r}') = \sum_i n_i\psi_i(\vec{r})\psi_i(\vec{r}')$ includes molecular orbitals ψ_i with nonzero occupancy n_i. The overlap distance $D(\vec{r})$ is the value of d maximizing EDR($\vec{r}$;d).[51] In this work we evaluate $D(\vec{r})$ on a molecule's density isosurface, similar to ESP. Distance $D(\vec{r})$ distinguishes compact *vs.* diffuse orbital lobes: it is modest for the single lobe of a hydrogen 1s orbital, small for the two lobes of a hydrogen 2p orbital, and large for the diffuse outer lobe of the lithium 2s orbital. $D(\vec{r})$ captures some effects of hybridization; regions with more p and d character tend to have smaller $D(\vec{r})$, while regions with more s character tend to give larger $D(\vec{r})$ (ESI,† Fig. S1). Density isosurface plots of $D(\vec{r})$ complement ESP surfaces and can capture trends in aromaticity, nucleophilicity, allotrope stability, substituent effects in metal clusters, selective binding of metal ions and ligands to enzymes, solvent softness, and can provide non-trivial predictions about chemical reactivity.[52–56] This work extends the applications of $D(\vec{r})$ and ESP molecular surfaces to aid the qualitative understanding of σ-holes. The quantitative analysis of these surfaces of isolated/free molecules provides a unique combination to predict σ-hole interaction strength.

2. Computational details

Calculations use the Gaussian 16[57] suite of programs. The systems shown in Fig. 1–4 utilize geometries optimized in the gas phase using density functional theory with the B3LYP[58–61] exchange–correlation functional and the def2-QZVP[62] basis set. The gas-phase halogen bond energies of ammonia with the systems shown in Fig. 1, were calculated using geometries of the complexes optimized at the MP2[63]/aug-cc-pVTZ[64] level (aug-cc-pVTZ-PP for iodine) with a counterpoise correction. The calculations for the Au nanocluster in Fig. 5 use coordinates from ref. 65 and compute the orbitals and energy at PW91PW91[66,67]/def2-SV(P)[68,69] DFT level. The calculations for systems mentioned in Fig. 6(a) use the B3PW91[67] functional and 6-31G(d,p)[70,71] basis set while Fig. 6(b) and (c) uses B3LYP/def2-TZVP[62] level of theory for the optimization of geometries. The Gaussian formatted checkpoint files are used to obtain electron density, ESP, and $D(\vec{r})$ grid data in the

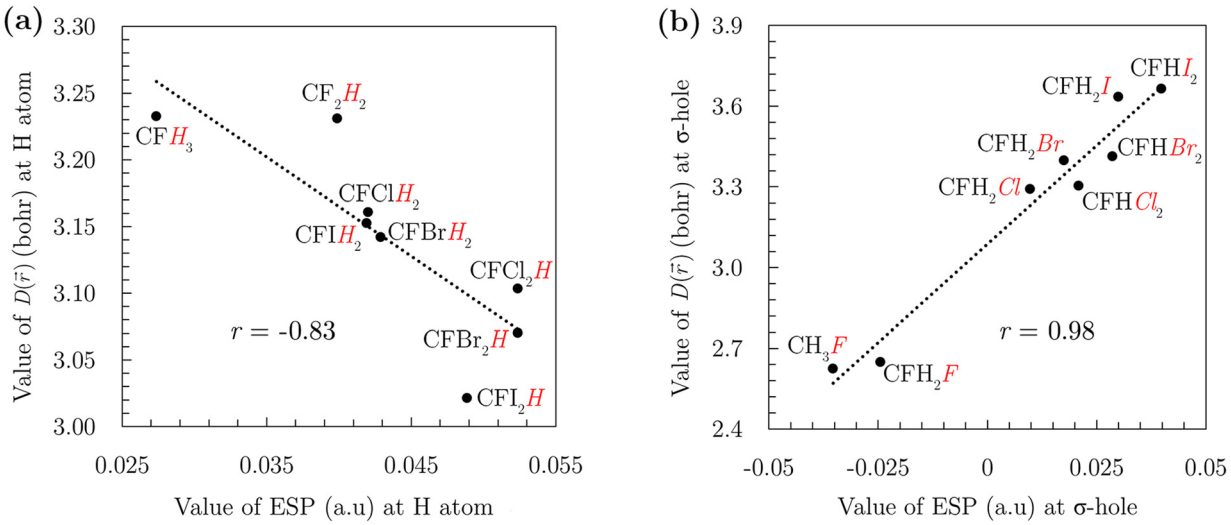

Fig. 2 Relation between molecular ESP and $D(\vec{r})$ evaluated on the and 0.001 e bohr^{-3} electron density isosurface of halomethanes (a) on H atom along the extension of C–H bond and (b) at the center of σ-hole of halogen atom shown in red (italic).

Gaussian cube file format using Multiwfn program.[72] For the calculations of $D(\vec{r})$, an even-tempered grid of 50 exponents is used starting from 2.50 bohr^{-2} and with an increment of 1.50 bohr^{-2}. For the studied systems, the calculated ESP and $D(\vec{r})$ cube files are projected over 0.001 e bohr^{-3} molecular electron density surface. The molecular graphics are created using VMD[73] version 1.9.3 and GaussView 5 package.

3. Results and discussion

Fig. 1 illustrates how the surface electrostatic potential and overlap distance combine to capture the chemistry of σ-holes. While ESP molecular surfaces effectively identify Lewis acidic sites as regions of electron deficiency relative to the surrounding molecule, $D(\vec{r})$ captures the local orbital character, distinguishing between diffuse and compact regions. This characterization reflects the local polarizability and provides a means to quantify the polarization contributions to σ-hole interactions. As a result, $D(\vec{r})$ offers complementary insights beyond those available from the ESP surface plots alone, highlighting information crucial for understanding the full nature of molecular interactions. For example, the Fig. 1 shows ESP and $D(\vec{r})$ computed for $CHFBr_2$ and CH_2FI. The ESP plots clearly show σ-holes on Br and I atoms. The isolated σ-hole donors have identical $V_{S,max}$, despite their different chemistry. The overlap distance captures those differences, clearly distinguishing the relatively compact σ-hole of Br in $CHFBr_2$ from the relatively diffuse σ-hole of I in CH_2FI. Fig. 2 shows how $D(\vec{r})$ captures the "special" chemistry of σ-holes. Typically, withdrawing electron density from a region leaves the remaining electron density to be held in more compact orbitals, such that more positive $V_{S,max}$ is correlated with smaller $D(\vec{r})$. The left panel of Fig. 2 illustrates this "typical" behavior for the H atom of halomethanes. In contrast, the right panel of Fig. 2 shows that for the same halomethanes, more positive $V_{S,max}$ at the σ-hole is correlated with larger $D(\vec{r})$. This is consistent with the explanation where a σ-hole arises when a half-filled p (or nearly p) orbital is involved in forming a covalent bond, leaving a region of depleted electron density. This depleted region has reduced p-type and enhanced s-type character, which is detected as a relatively large $D(\vec{r})$. In this sense, $D(\vec{r})$ captures the soft Lewis acid character of σ-holes. Before proceeding, it is important to emphasize that the magnitude of $D(\vec{r})$ in the σ-hole region remains largely unaffected by variations in basis sets or the choice of DFT exchange–correlation functionals. Tables S1 and S2 (ESI†) provide a detailed evaluation of $D(\vec{r})$ values for a range of σ-hole donors across different basis sets and electronic structure methods, confirming the minimal dependence of $D(\vec{r})$ on these computational parameters.

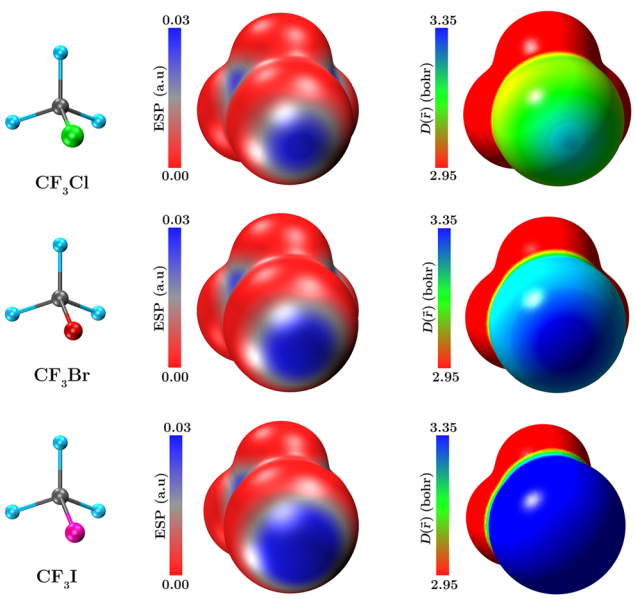

Fig. 3 σ-Holes on representative trifluorohalomethanes. (left) Molecule structure (middle-right) molecular ESP and $D(\vec{r})$ plotted on the and 0.001 e bohr^{-3} electron density isosurface.

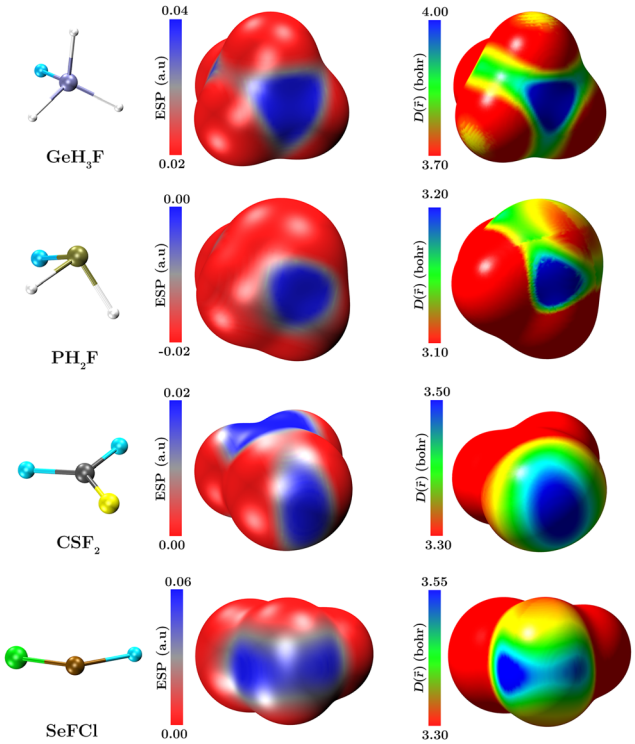

Fig. 4 σ-Holes on group p-valent IV–VI elements in representative molecules. (left) Molecule structure (middle-right) molecular ESP and $D(\vec{r})$ plotted on the and 0.001 e bohr^{-3} electron density isosurface.

Fig. 3 shows the optimized structures, and calculated ESP and $D(\vec{r})$ surface plots of trifluorohalomethanes and confirms the general understanding that the magnitude of σ-holes, hence their acidic strength, increases with the increased atomic number down the group. The $D(\vec{r})$ surface plots show that σ-hole regions of halogens have large values of $D(\vec{r})$ and are more diffuse relative to the other regions of the atom. With a decrease in electronegativity and an increase in polarizability, the values of $D(\vec{r})$ increase down the group with more diffuse σ-hole of trifluoroiodomethane have a region with the largest value of $D(\vec{r})$ while σ-hole of trifluorochloromethane has a

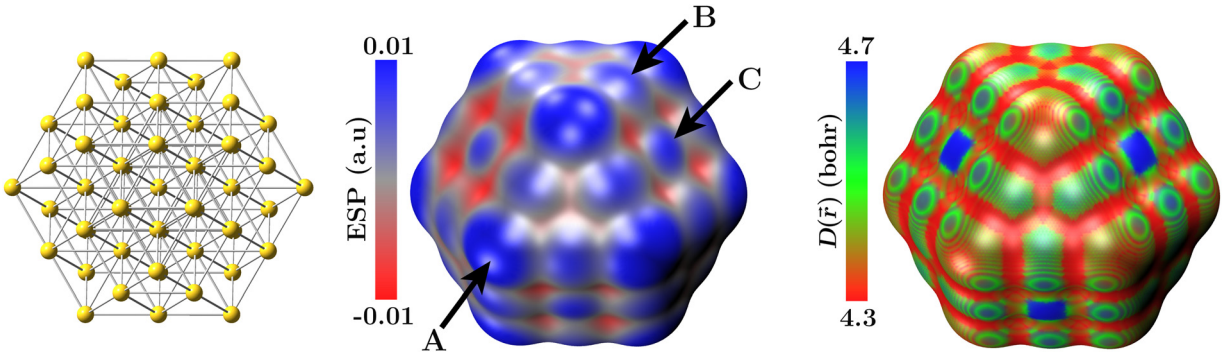

Fig. 5 σ-Holes on Au_{55} nanocluster. (left) Gas-phase structure (middle) molecular ESP and (right) $D(\vec{r})$ plotted on the and 0.001 e bohr^{-3} electron density isosurface. The overlap distance $D(\vec{r})$ clearly distinguishes the "true" σ-holes C from the other positively charged regions.

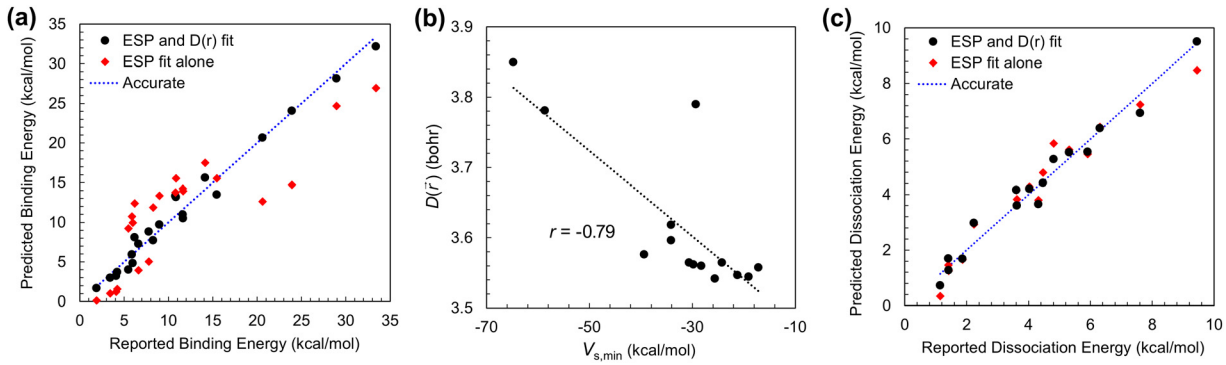

Fig. 6 (a) Relation between reported and predicted binding energies using $V_{S,min}$ and $D(\vec{r})$ (black circles) and $V_{S,min}$ alone (red diamonds), for F–Cl complexes with CN–R and SiN–R acceptors evaluated on acceptor C or Si atoms. (b) Relation between $V_{S,min}$ and $D(\vec{r})$ for the CN–R complexes, and (c) relation between reported and predicted dissociation energies of NCH acceptor from XB18 and XB51 datasets using $V_{S,max}$ and $D(\vec{r})$ (black circles) and $V_{S,max}$ alone (red diamonds). Tables S3–S6 (ESI†) provides the values for individual systems.

localized disc shape region with a relatively small value of $D(\vec{r})$. These findings suggest that the chemical softness of σ-hole increases down the group with a corresponding increase in their acidic strengths. Besides, for all halomethanes, the negative ESP, *i.e.*, nucleophilic or basic regions surrounding the σ-holes are relatively compact indicated by their small $D(\vec{r})$ relative to the σ-hole, which suggests that these regions are relatively hard-basic sites. The hardness of these regions decreases down the group with an increase in the magnitude and size of σ-holes.

The σ-hole concept has been extended to a broad range of systems, including chalcogen and pnictogen bonding as well as transition metals.[2,48,65,74–83] We have systematically studied the overlap distance in these systems. Fig. 4 depicts the location and characteristics of σ-holes through ESP and $D(\vec{r})$ density isosurface plots for a selection of molecules containing p-valent group IV–VI elements. The number of σ-holes observed corresponds to the number of covalent bonds formed by the central atom. In the case of GeH_3F, the triangular σ-hole is positioned along the extension of the F–Ge bond, at the intersection of the three H–Ge bonds, as revealed by the ESP surface plot. While σ-holes arising from H–Ge bonds also extend along their bond axes, only one such σ-hole is partially visible in Fig. 4 due to the molecular orientation selected. Unlike σ-holes associated with halogens, where negative ESP regions typically surround the central atom, the σ-hole on the Ge atom in GeH_3F is characterized solely by a region of positive ESP. The $D(\vec{r})$ isosurface plot further corroborates the ESP findings, highlighting the σ-hole as a triangular feature with a diffuse nature, represented by a green ribbon with elevated $D(\vec{r})$ values. Similarly, in PH_2F, a σ-hole appears along the extension of the F–P bond, as seen in the ESP plot. However, the σ-holes formed by the H–P bonds are obscured due to the dominant negative ESP region associated with the P atoms lone pairs. Again, the $D(\vec{r})$ plot captures the σ-hole, displaying it as a diffuse triangular feature with a corresponding high $D(\vec{r})$ value. In the case of CSF_2, sulfur, being divalent, forms a double bond with carbon, resulting in a single oval-shaped σ-hole on the sulfur atom, as illustrated by the ESP surface plot. This σ-hole is notably diffuse, with a large $D(\vec{r})$ value, indicating its soft-acidic nature. For SeFCl, the Se atom exhibits two σ-holes, aligned along the extensions of the F–Se and Cl–Se bonds. The influence of the electronegativity difference between F and Cl is evident in the magnitude and size of the σ-holes, with the F-induced σ-hole being larger and more intense than that induced by Cl. This contrast is further emphasized in the $D(\vec{r})$ plot, where the σ-hole associated with

F is notably more diffuse compared to that of Cl. These results suggest that σ-holes in group IV–VI elements, arising from valence p-orbitals, are characterized by extensive $D(\vec{r})$ regions, highlighting their role as soft-acidic sites in molecular interactions. While ESP surface plots effectively pinpoint σ-hole locations, $D(\vec{r})$ isosurfaces provide critical insight into their diffuse or compact nature, largely mirroring trends observed in Fig. 1–3: more polarizable atoms tend to have larger $D(\vec{r})$ on the σ-hole and there is an unusual positive correlation between σ-hole $V_{S,max}$ and $D(\vec{r})$. Fig. 5 illustrates representative results, showing how $D(\vec{r})$ can distinguish so-called ''true σ-holes'' from ''pseudo-σ-holes'' (or σ_s-holes arising from electron deficiencies in the valence s-orbitals as categorized in ref. 48) in transition metal nanoclusters. Fig. 5 shows the surface ESP and $D(\vec{r})$ plots of low energy, cuboctahedra Au_{55} nanoclusters. The ESP positive values follow the previously reported trend[65] of corners (A) > edges (B) > facets (C) which complement their catalytic activity order.[65] Previous studies have suggested that the ''true σ-holes'' characterized by $V_{S,max}$ deviates from the typical lateral extension of the Au–Au bond.[48] The $D(\vec{r})$ plot clearly distinguishes these sites as having the largest $D(\vec{r})$, detecting and confirming their identity as ''true σ-holes'' as distinct from the remaining ''pseudo-σ-holes''.[48]

We continue by demonstrating that combining the ESP and overlap distance of isolated halogen bond donors and acceptors can better quantify their interaction energies. We begin with the F–Cl···CN–R and F–Cl···SiN–R complexes studied by Politzer *et al.*,[9] where R = CN, NC, NO_2, F, CF_3, Cl, Br, H, CCF, CCH, CH_3, SiH_3, Li, Na, F, Cl. These authors found that $V_{S,min}$ of the σ-hole acceptor (Lewis base) C and Si atoms of CN–R and SiN–R were not perfectly correlated with halogen bond energies and used the local ionization energy to improve the model.[9] We instead combine the isolated σ-hole acceptor's $V_{S,min}$ (kcal mol^{-1}) with $D(\vec{r})$ evaluated at that same point. We fit the binding energies computed by Politzer *et al.*, to eqn (2),

$$\text{B.E.} = \alpha D(\vec{r}) - \beta V_{S,min} - \gamma \quad (2)$$

(Individual $D(\vec{r})$ and $V_{S,min}$ are in Table S3, ESI.†) The fit reproduces the binding energies with R^2 = 0.98, RMS error of 1.31 kcal mol^{-1}, $\alpha = 13 \pm 1$ kcal mol^{-1} $bohr^{-1}$, $\beta = 0.51 \pm 0.02$ and $\gamma = 52 \pm 4$ kcal mol^{-1}. These errors are comparable to those reported by Politzer *et al.* (R^2 = 0.987, RMS error of 1.02 kcal mol^{-1}),[9] from the local ionization energy. Fig. 6(a) (black circles) shows the correlation between the reported binding energies and those predicted from eqn (2). Fitting ESP alone (α = 0, Fig. 6(a) red diamonds) reduces R^2 to 0.71 and increases the RMS error to 4.61 kcal mol^{-1}. Fig. 6(b) illustrates the relationship between $D(\vec{r})$ and $V_{S,min}$ for the CN–R complexes. While these descriptors exhibit a moderate correlation ($r = -0.79$), the interaction energies predicted using eqn (2) show excellent agreement with the reported values. This result indicates that $D(\vec{r})$ offers additional, complementary insights into the R-group dependence of CN–R halogen bond strengths. As a ''sanity test'', we also modeled complexes F–Br···X–R, X = F, Cl, Br, I and R = –H, –F, where $V_{S,min}$ alone is known to be more predictive. Table S4 and Fig. S5 (ESI†) shows that adding the $D(\vec{r})$ values modestly improve the fit, R^2 = 0.88 and RMS error of 0.53 kcal mol^{-1}.

We conclude by predicting the dissociation and interaction energies of a diverse range of halogen-bonded complexes, utilizing the $V_{S,max}$ and $D(\vec{r})$ of the isolated σ-hole donors. As discussed above, $V_{S,max}$ of the isolated halogen bond donors was not predictive of interaction/dissociation energies (E), however $V_{S,max}$ of the donor perturbed by a point charge at the acceptor position gave quite accurate results. We hypothesize that $D(\vec{r})$ of the isolated halogen bond donors would capture aspects of their response properties, and used eqn (3) to fit the model.

$$E = \alpha D(\vec{r}) + \delta V_{S,max} + \kappa V_{S,max} D(\vec{r}) + \gamma \quad (3)$$

We fitted the interaction energies from the X40 dataset[84] for the binding of a single σ-hole acceptor, formaldehyde, with six different halogen bond donors (CH_3X and CF_3X, where X = Cl, Br, I). The fit to the equation yielded the parameters: $\alpha = -1.210 \pm 1.380$ kcal mol^{-1} $bohr^{-1}$, $\delta = -0.425 \pm 0.255$, $\kappa = 0.148 \pm 0.075$ $bohr^{-1}$, and $\gamma = 5.23 \pm 4.64$ kcal mol^{-1}. Notably, eqn (3) only utilizes information from the isolated σ-hole donors and does not require details of the complex geometry or the acceptor's characteristics. The fit in Fig. S6 (ESI†) demonstrates a strong correlation (black circles in Fig. S6, ESI†) between the reported interaction energies and those predicted by eqn (3), with an R^2 of 0.98 and a root mean square (RMS) error of 0.29 kcal mol^{-1}. However, fitting only $V_{S,max}$ (red diamonds in Fig. S6, ESI†) reduces the R^2 to 0.93 and increases the RMS error to 0.61 kcal mol^{-1}.

Similarly, the dissociation energies for σ-hole donors with an NCH acceptor from the XB18 and XB51 datasets[85] were predicted using the same model (eqn (3)). The fitting yielded $\alpha = -3.09 \pm 0.30$ kcal mol^{-1} $bohr^{-1}$, $\delta = -0.359 \pm 0.217$, $\kappa = 0.147 \pm 0.061$ $bohr^{-1}$, and $\gamma = 9.97 \pm 8.08$ kcal mol^{-1}. As shown in Fig. 6(c), the correlation between the reported dissociation energies and those predicted by eqn (3) is high (black circles), with an R^2 of 0.97 and an RMS error of 1.6 kcal mol^{-1}. Again, fitting $V_{S,max}$ alone (red diamonds in Fig. 6(c)) resulted in a lower R^2 of 0.95 and an increased RMS error of 2.1 kcal mol^{-1}. In future work, we plan to extend the current model to analyze large datasets of σ-hole interaction energies, such as SH250x10.[86] This will be detailed in subsequent publications.

4. Conclusions

Our $D(\vec{r})$ surface plots complement the ESP surfaces and provide a comprehensive picture of σ-holes and related interactions. The $D(\vec{r})$ surfaces can be used to categorize a σ-hole as diffuse or compact, which may help to rationalize them as a hard or soft chemical center. The combination of $D(\vec{r})$ and ESP can be equally used to predict the strength of σ-holes or halogen bonding interactions. These tools are available freely in Multiwfn[72] wavefunction analysis package and also in Gaussian 16.[57]

Author contributions

Arshad Mehmood conceived the project idea, conducted calculations, analyzed data, and drafted the initial manuscript. Benjamin G. Janesko supervised the project, provided guidance throughout the research process, and contributed to the writing of the original draft. Both authors critically reviewed and approved the final version of the manuscript for publication.

Data availability

The data supporting this article have been included as part of the ESI.†

Conflicts of interest

There are no conflicts to declare.

References

1 T. Brinck, J. S. Murray and P. Politzer, *Int. J. Quantum Chem.*, 1992, **44**, 57–64.
2 M. H. Kolar and P. Hobza, *Chem. Rev.*, 2016, **116**, 5155–5187.
3 T. Clark, M. Hennemann, J. S. Murray and P. Politzer, *J. Mol. Model.*, 2007, **13**, 291–296.
4 B. Mallada, A. Gallardo, M. Lamanec, B. de la Torre, V. Špirko, P. Hobza and P. Jelinek, *Science*, 2021, **374**, 863–867.
5 F. Heinen, D. L. Reinhard, E. Engelage and S. M. Huber, *Angew. Chem., Int. Ed.*, 2021, **60**, 5069–5073.
6 F. Heinen, E. Engelage, C. J. Cramer and S. M. Huber, *J. Am. Chem. Soc.*, 2020, **142**, 8633–8640.
7 P. Politzer, J. S. Murray and T. Clark, *Phys. Chem. Chem. Phys.*, 2013, **15**, 11178–11189.
8 P. Metrangolo, J. S. Murray, T. Pilati, P. Politzer, G. Resnati and G. Terraneo, *Cryst. Growth Des.*, 2011, **11**, 4238–4246.
9 P. Politzer and J. S. Murray, *Theor. Chem. Acc.*, 2012, **131**, 1114.
10 A. Mukherjee, S. Tothadi and G. R. Desiraju, *Acc. Chem. Res.*, 2014, **47**, 2514–2524.
11 P. Politzer and J. S. Murray, *Chem. Phys. Chem.*, 2013, **14**, 278–294.
12 A. Bundhun, P. Ramasami, J. S. Murray and P. Politzer, *J. Mol. Model.*, 2013, **19**, 2739–2746.
13 K. E. Riley, J. S. Murray, J. Fanfrlík, J. Řezáč, R. J. Solá, M. C. Concha, F. M. Ramos and P. Politzer, *J. Mol. Model.*, 2011, **17**, 3309–3318.
14 K. E. Riley, J. S. Murray, P. Politzer, M. C. Concha and P. Hobza, *J. Chem. Theory Comput.*, 2009, **5**, 155–163.
15 P. Politzer, J. S. Murray and M. C. Concha, *J. Mol. Model.*, 2008, **14**, 659–665.
16 K. Eskandari and M. Lesani, *Chem. – Eur. J.*, 2015, **21**, 4739–4746.
17 J. S. Murray and P. Politzer, *Crystals*, 2020, **10**, 1–16.
18 T. Clark, P. Politzer and J. S. Murray, *WIREs Comput. Mol. Sci.*, 2015, **5**, 169–177.
19 D. J. R. Duarte, G. L. Sosa, N. M. Peruchena and I. Alkorta, *Phys. Chem. Chem. Phys.*, 2016, **18**, 7300–7309.
20 J. Thirman, E. Engelage, S. M. Huber and M. Head-Gordon, *Phys. Chem. Chem. Phys.*, 2018, **20**, 905–915.
21 T. Clark and A. HeÃŸelmann, *Phys. Chem. Chem. Phys.*, 2018, **20**, 22849–22855.
22 S. M. Huber, E. Jimenez-Izal, J. M. Ugalde and I. Infante, *Chem. Commun.*, 2012, **48**, 7708–7710.
23 A. Varadwaj, H. M. Marques and P. R. Varadwaj, *Molecules*, 2019, **24**, 379.
24 L. P. Wolters and F. M. Bickelhaupt, *ChemistryOpen*, 2012, **1**, 96–105.
25 S. V. Rosokha, C. L. Stern and J. T. Ritzert, *Chem. – Eur. J.*, 2013, **19**, 8774–8788.
26 B. Pinter, N. Nagels, W. A. Herrebout and F. DeProft, *Chem. – Eur. J.*, 2013, **19**, 519–530.
27 S. M. Huber, J. D. Scanlon, E. Jimenez-Izal, J. M. Ugalde and I. Infante, *Phys. Chem. Chem. Phys.*, 2013, **15**, 10350–10357.
28 L. P. Wolters, P. Schyman, M. J. Pavan, W. L. Jorgensen, F. M. Bickelhaupt and S. Kozuch, *Wiley Interdiscip. Rev.: Comput. Mol. Sci.*, 2014, **4**, 523–540.
29 C. Wang, D. Danovich, Y. Mo and S. Shaik, *J. Chem. Theory Comput.*, 2014, **10**, 3726–3737.
30 L. P. Wolters, N. W. G. Smits and C. F. Guerra, *Phys. Chem. Chem. Phys.*, 2015, **17**, 1585–1592.
31 S. W. Robinson, C. L. Mustoe, N. G. White, A. Brown, A. L. Thompson, P. Kennepohl and P. D. Beer, *J. Am. Chem. Soc.*, 2015, **137**, 499–507.
32 V. Oliveira, E. Kraka and D. Cremer, *Phys. Chem. Chem. Phys.*, 2016, **18**, 33031–33046.
33 V. Oliveira, E. Kraka and D. Cremer, *Inorg. Chem.*, 2017, **56**, 488–502.
34 O. Grounds, M. Zeller and S. V. Rosokha, *New J. Chem.*, 2018, **42**, 10572–10583.
35 V. Angarov and S. Kozuch, *New J. Chem.*, 2018, **42**, 1413–1422.
36 S. J. Ang, A. M. Mak and M. W. Wong, *Phys. Chem. Chem. Phys.*, 2018, **20**, 26463–26478.
37 E. Rossi, M. De Santis, D. Sorbelli, L. Storchi, L. Belpassi and P. Belanzoni, *Phys. Chem. Chem. Phys.*, 2020, **22**, 1897–1910.
38 A. Varadwaj, P. R. Varadwaj, H. M. Marques and K. Yamashita, *Phys. Chem. Chem. Phys.*, 2018, **20**, 15316–15329.
39 T. Clark, J. S. Murray and P. Politzer, *Phys. Chem. Chem. Phys.*, 2018, **20**, 30076–30082.
40 P. V. Bijina and C. H. Suresh, *J. Phys. Chem. A*, 2020, **124**, 2231–2241.
41 S. Scheiner, *J. Phys. Chem. A*, 2020, **124**, 7290–7299.
42 T. Clark and M. G. Hicks, *Beilstein J. Org. Chem.*, 2020, **16**, 1649–1661.
43 Z. Zhu, Z. Xu and W. Zhu, *J. Chem. Inf. Model.*, 2020, **60**, 2683–2696.
44 E. Engelage, D. Reinhard and S. M. Huber, *Chem. – Eur. J.*, 2020, **26**, 3843–3861.
45 M. A. A. Ibrahim and A. A. M. Hasb, *Theor. Chem. Acc.*, 2018, **138**, 2.
46 J. S. Murray and P. Politzer, *J. Indian Inst. Sci.*, 2020, **100**, 21–30.
47 T. Brinck and A. N. Borrfors, *J. Mol. Model.*, 2019, **25**, 125.

48 J. H. Stenlid, A. J. Johansson and T. Brinck, *Crystals*, 2017, **7**, 222.
49 O. A. Syzgantseva, V. Tognetti and L. Joubert, *J. Phys. Chem. A*, 2013, **117**, 8969–8980.
50 S. J. Grabowski, *J. Phys. Chem. A*, 2012, **116**, 1838–1845.
51 B. G. Janesko, G. Scalmani and M. J. Frisch, *J. Chem. Phys.*, 2014, **141**, 144104.
52 A. Mehmood and B. G. Janesko, *Angew. Chem., Int. Ed.*, 2017, **56**, 6878–6881.
53 A. Mehmood, S. I. Jones, P. Tao and B. G. Janesko, *J. Chem. Inf. Model.*, 2018, **58**, 1836–1846.
54 B. G. Janesko, K. B. Wiberg, G. Scalmani and M. J. Frisch, *J. Chem. Theory Comput.*, 2016, **12**, 3185–3194.
55 A. Mehmood, S. I. Jones, P. Tao and B. G. Janesko, *J. Chem. Inf. Model.*, 2018, **58**, 1836–1846.
56 A. Mehmood and B. G. Janesko, *J. Solution Chem.*, 2020, **49**, 614–628.
57 M. J. Frisch, G. W. Trucks, H. B. Schlegel, G. E. Scuseria, M. A. Robb, J. R. Cheeseman, G. Scalmani, V. Barone, G. A. Petersson, H. Nakatsuji, X. Li, M. Caricato, A. V. Marenich, J. Bloino, B. G. Janesko, R. Gomperts, B. Mennucci, H. P. Hratchian, J. V. Ortiz, A. F. Izmaylov, J. L. Sonnenberg, D. Williams-Young, F. Ding, F. Lipparini, F. Egidi, J. Goings, B. Peng, A. Petrone, T. Henderson, D. Ranasinghe, V. G. Zakrzewski, J. Gao, N. Rega, G. Zheng, W. Liang, M. Hada, M. Ehara, K. Toyota, R. Fukuda, J. Hasegawa, M. Ishida, T. Nakajima, Y. Honda, O. Kitao, H. Nakai, T. Vreven, K. Throssell, J. A. Montgomery Jr., J. E. Peralta, F. Ogliaro, M. J. Bearpark, J. J. Heyd, E. N. Brothers, K. N. Kudin, V. N. Staroverov, T. A. Keith, R. Kobayashi, J. Normand, K. Raghavachari, A. P. Rendell, J. C. Burant, S. S. Iyengar, J. Tomasi, M. Cossi, J. M. Millam, M. Klene, C. Adamo, R. Cammi, J. W. Ochterski, R. L. Martin, K. Morokuma, O. Farkas, J. B. Foresman and D. J. Fox, *Gaussian 16 Rev. C.01*, 2016.
58 A. D. Becke, *J. Chem. Phys.*, 1993, **98**, 5648–5652.
59 C. Lee, W. Yang and R. G. Parr, *Phys. Rev. B: Condens. Matter Mater. Phys.*, 1988, **37**, 785.
60 S. H. Vosko, L. Wilk and M. Nusair, *Can. J. Phys.*, 1980, **58**, 1200–1211.
61 P. J. Stephens, F. J. Devlin, C. F. Chabalowski and M. J. Frisch, *J. Phys. Chem.*, 1994, **98**, 11623–11627.
62 F. Weigend, F. Furche and R. Ahlrichs, *J. Chem. Phys.*, 2003, **119**, 12753–12762.
63 C. Møller and M. S. Plesset, *Phys. Rev.*, 1934, **46**, 618–622.
64 A. K. Wilson, D. E. Woon, K. A. Peterson and T. H. Dunning Jr, *J. Chem. Phys.*, 1999, **110**, 7667–7676.
65 J. H. Stenlid and T. Brinck, *J. Am. Chem. Soc.*, 2017, **139**, 11012–11015.
66 J. P. Perdew, J. A. Chevary, S. H. Vosko, K. A. Jackson, M. R. Pederson, D. J. Singh and C. Fiolhais, *Phys. Rev. B: Condens. Matter Mater. Phys.*, 1992, **46**, 6671–6687.
67 J. P. Perdew, *Electronic Structure of Solids*, 1991, Akademie Verlag, Berlin.
68 D. Andrae, U. HäuÃŸermann, M. Dolg, H. Stoll and H. PreuÃŸ, *Theoretica Chimica Acta*, 1990, **77**, 123–141.
69 F. Weigend and R. Ahlrichs, *Phys. Chem. Chem. Phys.*, 2005, **7**, 3297–3305.
70 P. C. Hariharan and J. A. Pople, *Theor. Chim. Acta*, 1973, **28**, 213–222.
71 W. J. Hehre, R. Ditchfield and J. A. Pople, *J. Chem. Phys.*, 1972, **56**, 2257–2261.
72 T. Lu and F. Chen, *J. Comput. Chem.*, 2012, **33**, 580–592.
73 W. Humphrey, A. Dalke and K. Schulten, *J. Mol. Graphics*, 1996, **14**, 33–38.
74 J. Y. C. Lim and P. D. Beer, *Chem*, 2018, **4**, 731–783.
75 W. Wang, B. Ji and Y. Zhang, *J. Phys. Chem. A*, 2009, **113**, 8132–8135.
76 M. E. Brezgunova, J. Lieffrig, E. Aubert, S. Dahaoui, P. Fertey, S. Lebègue, J. G. Ángyán, M. Fourmigué and E. Espinosa, *Cryst. Growth Des.*, 2013, **13**, 3283–3289.
77 J. E. Del Bene, I. Alkorta, G. Sanchez-Sanz and J. Elguero, *J. Phys. Chem. A*, 2011, **115**, 13724–13731.
78 S. Zahn, R. Frank, E. Hey-Hawkins and B. Kirchner, *Chem. – Eur. J.*, 2011, **17**, 6034–6038.
79 S. Scheiner, *Acc. Chem. Res.*, 2013, **46**, 280–288.
80 A. Bauzá, T. J. Mooibroek and A. Frontera, *Angew. Chem., Int. Ed.*, 2013, **52**, 12317–12321.
81 M. A. A. Ibrahim, R. R. A. Saeed, M. N. I. Shehata, N. A. M. Moussa, A. M. Tawfeek, M. N. Ahmed, M. K. Abd El-Rahman and T. Shoeib, *ACS Omega*, 2023, **8**, 32828–32837.
82 A. Amonov and S. Scheiner, *Phys. Chem. Chem. Phys.*, 2023, **25**, 23530–23537.
83 A. Friedrich, J. Pahl, J. Eyselein, J. Langer, N. van Eikema Hommes, A. Görling and S. Harder, *Chem. Sci.*, 2021, **12**, 2410–2418.
84 J. Rezáč, K. E. Riley and P. Hobza, *J. Chem. Theory Comput.*, 2012, **8**, 4285–4292.
85 S. Kozuch and J. M. L. Martin, *J. Chem. Theory Comput.*, 2013, **9**, 1918–1931.
86 K. Kříž and J. Řezáč, *Phys. Chem. Chem. Phys.*, 2022, **24**, 14794–14804.